# Electrochemical Study of Interfacial Composite Nanostructures: Polyelectrolyte/Gold Nanoparticle Multilayers Assembled on Phospholipid/Dextran Sulfate Monolayers at a Liquid−Liquid Interface

**Hélder A. Santos,*,† Mariana Chirea,§ Vladimir García-Morales,‡ Fernando Silva,§ José A. Manzanares,‡ and Kyösti Kontturi*,†**

*Department of Chemical Technology, Laboratory of Physical Chemistry and Electrochemistry, Helsinki University of Technology, P.O. Box 6100, FIN-02015 HUT, Finland; Departamento de Química, Faculdade de Ciências, Universidade do Porto, Rua do Campo Alegre 687, 4169-007 Porto, Portugal; Departament de Termodinàmica, Universitat de València, E−46100 Burjassot, Spain*

*Received: May 12, 2005; In Final Form: August 22, 2005*

The build up and electrochemical characterization of interfacial composite nanostructures containing a cationic polyelectrolyte and negatively charged mercaptosuccinic acid stabilized gold nanoparticles (AuNPs) is reported. The nanostructures were formed at the interface between two immiscible electrolyte solutions in which the organic phase is an immobilized 2-nitrophenyl octyl ether/PVC gel. The growth of the multilayer was verified with UV−vis spectra, and approximately a linear increase in UV−vis absorbance with increasing number of layers was observed. The interfacial capacitance of the multilayers was measured as a function of the potential and a theoretical model was developed to explain the results. The excellent agreement between theoretical and experimental capacitance curves allows us to conclude that nanocomposites behave similarly to polyelectrolyte multilayers, with the outmost layer determining the alternating sign of the outer surface charge density. Cyclic voltammograms were used to evaluate the transfer rate constant across the multilayers of a model drug, metoprolol, and the standard probe tetraethylammonium cation. The apparent rate constants were slightly larger than in other studies in the literature and decrease with the increasing number of layers.

## Introduction

Nanoparticle assemblies are of great interest because of their potential applications in different fields such as semiconductors, molecular electronics, photovoltaic cells, chemical and biological sensing, and catalysis.[1,2] In particular, the research on polyelectrolyte/metal nanoparticles self-assembled multilayers[3] has increased significantly,[4−10] as they can be used, among other things, to fabricate nanocomposites and nanopatterning materials fundamental for delivery devices. For example, microcapsules can be fabricated by layer-by-layer (LbL) technique by alternatively adsorbing oppositely charged polyelectrolytes on metal nanoparticles, containing in their interior materials such as polymers, enzymes, drugs, etc., making them very suitable as potential delivery vesicles. Therefore, a system made of complexed biomimetic thin films (lipid + biopolymer + polyelectrolyte + nanoparticles) could be used for the construction of a biosensor for the monitoring, for example, of controlled-release and targeting sites of such capsules in biological cells.

A fundamental prerequisite for the use of nanoparticles in biological applications is that they should be easily dispersible in water because they must combine with macromolecules in aqueous solution.[11] Using the method of Chen and Kimura,[12] negatively charged and water-soluble gold nanoparticles (AuNPs) with the size distribution between 1 and 3 nm can be obtained. Also, these AuNPs can be precipitated and redispersed in water without further aggregation, which represents an advantage compared with other aqueous gold colloids that suffer from easy aggregation.[13−16]

The interaction of macromolecules of biological interest with lipid membranes is important in various areas such as membrane biophysics[17−19] and drug formulations. Many studies on lipid monolayers at the air−liquid[20−23] interface and at the interface between two immiscible electrolytes solutions[22] (ITIES) have been reported to obtain information about ion[22,24−28] and drug transfer[22,29−31] across a single monolayer or across hybrid systems containing also different polyelectrolyte layers.

In this work, we study composite multilayers containing a cationic polyelectrolyte and negatively charged mercaptosuccinic acid stabilized AuNPs at a biomimetic lipid membrane. In particular, a monolayer of the positively charged phospholipid *N*-[1-(2,3-dioleoyloxy)-propyl]-*N*,*N*,*N*-trimethylammonium chloride (DOTAP) at an ITIES was used as a model membrane, and negatively charged dextran sulfate (DS) was used as the model for glycosaminoglycans (GAGs).[21−23] GAGs, consisting of highly sulfated and negatively charged polysaccharides, are the major components in the extracellular matrixes of many tissues, and they can also be found inside the cells. DS is a good model for the GAGs because of their structural similarity, and in addition, it has been found that DS might carry out an important role as an anti-atherosclerotic drug,[32] anti-HIV infection agent,[33] and more recently, in gene delivery systems.[34−36]

The hybrid layer is formed at the air−water interface in a Langmuir trough by electrostatic absorption of DS present in the subphase to the DOTAP monolayer. The interaction between DS and the DOTAP monolayer is followed, measuring the

* Corresponding author. E-mail: helder.santos@hut.fi (H.A.S.); kontturi@cc.hut.fi (K.K.). Telephone: +358 9 451 2570. Fax: +358 9 451 2580.

† Helsinki University of Technology.

‡ Universitat de València.

§ Universidade do Porto.

10.1021/jp052485p CCC: $30.25 
Published on Web 10/01/2005

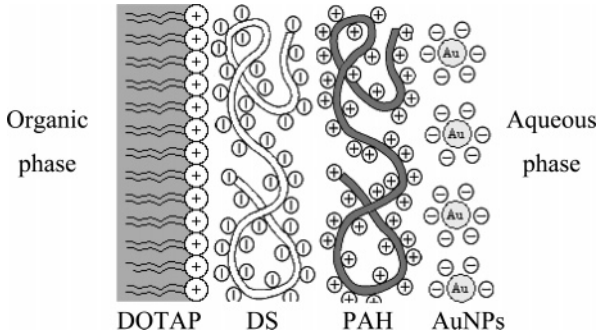


**Figure 1.** Schematic representation of a DOTAP/DS/PAH/AuNPs interfacial composite nanostructure.

compression isotherms. The hybrid layer is then transferred at a surface pressure of 32 mN/m by using the Langmuir−Blodgett (LB) technique[37−41] onto the organic gel. The growth of the polyelectrolyte/AuNPs is achieved by immersing the gel/hybrid layer assembly alternatively in aqueous solutions of cationic poly(allylamine hydrochloride) (PAH) and anionic AuNPs and is followed by UV−vis spectroscopy. The nanoparticle concentration in the solution is 0.06 mg/mL, and two different size distributions, with average diameters of 1.7 and 2.9 nm, are used separately.

The interfacial nanostructures are characterized by AC and cyclic voltammetry. The capacitance curves measured by AC voltammetry provide information on the electrical structure of these interfacial nanocomposites. The capacitance curves are analyzed with the help of a theoretical model describing the electrical potential distribution at all stages of the multilayer growth. Cyclic voltammetry is used to estimate the rate of transfer of tetraethylammonium ($TEA^+$) and the cationic $\beta$-blocker, metoprolol, across the multilayers as a function of the number of layers and nanoparticle size.

## Theory

The interfacial composite nanostructures under study are depicted in Figure 1. All nanostructures contain the DOTAP/DS hybrid layer and differ in the number of alternating PAH and AuNPs layers. We use $n$ for the number of PAH and AuNPs layers, and therefore, the system in Figure 1 corresponds to $n = 2$. We present first a relatively simple theoretical model to evaluate the capacitance $C$ of the interfacial nanostructure. This is defined as

$$C \equiv \frac{\partial Q}{\partial \Delta_o^w \phi} \tag{1}$$

where $Q$ is the charge density separated across the ITIES, and $\Delta_o^w\phi \equiv \phi_w^b - \phi_o^b$ is the Galvani potential difference between the bulk aqueous and organic phases. The interfacial nanostructure is described by using a one-dimensional model in which the ITIES is located at the plane $x = 0$, the organic gel occupies the region $x < 0$, and the aqueous solution the region $x > 0$. The organic and aqueous bulk phases (i.e., the regions outside the electrical double layer at the ITIES) have molar concentrations of their respective 1:1 base electrolytes $c_o^b$ and $c_w^b$, and relative electrical permittivities $\epsilon_o$ and $\epsilon_w$, respectively.

The hydrocarbon chains of the phospholipids occupy the region $-d_{hc} < x < 0$, which is characterized by a relative permittivity $\epsilon_{hc}$. The different permittivity of the hydrocarbon region and the organic phase implies that a chemical partition coefficient $K_{hc}$ needs to be included when describing the spatial

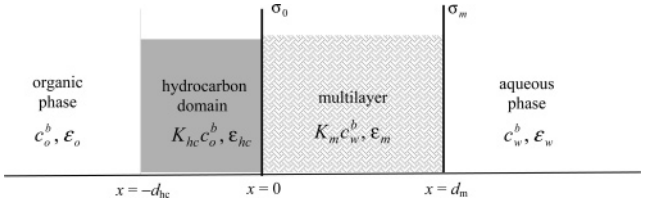


**Figure 2.** Schematic representation of the interfacial system.

distribution of the organic base electrolyte, and hence its effective concentration in the hydrocarbon region is $c_{hc}^b = K_{hc} c_o^b$. The composite PAH/AuNPs multilayer is modeled as a single phase that occupies the region $0 < x < d_m$ and has relative permittivity $\epsilon_m$. Again, partitioning effects are important, and the effective concentration of the aqueous base electrolyte in this region is $c_m^b = K_m c_w^b$, where $K_m$ is their chemical partition coefficient.

The charges bound to this interfacial nanostructure are modeled as two plane distributions at $x = 0$ and $x = d_m$ (see Figure 2). The respective electrical charge densities are $\sigma_0$ and $\sigma_m$ or, in dimensionless units, $\alpha \equiv A\sigma_0/e$ and $\gamma \equiv A\sigma_m/e$ where $e$ is the elementary charge and $A$ is the mean molecular area of the phospholipids in the monolayer.

The electric potential distribution in region $i$ ($i$ = o, hc, m, w) is described by the Poisson−Boltzmann equation[24]

$$\frac{d^2\varphi}{dx^2} = \kappa_i^2 \sinh(\varphi - \varphi_i^b) \tag{2}$$

where $\varphi \equiv F(\phi - \phi_o^b)/RT$ is the dimensionless electric potential, $\varphi_m^b \equiv \varphi_w^b$, $\varphi_{hc}^b \equiv \varphi_o^b = 0$,

$$\kappa_i \equiv \left(\frac{2F^2 c_i^b}{\epsilon_i \epsilon_0 RT}\right)^{1/2} \tag{3}$$

is the Debye parameter in region $i$, and $\epsilon_0$ is the vacuum electrical permittivity. Multiplying eq 2 by $2d\varphi/dx$, it can be integrated to

$$\frac{d\varphi}{dx} = \pm\left[\kappa_i^2 \sinh^2\left(\frac{\varphi - \varphi_i^b}{2}\right) + a_i\right]^{1/2} \tag{4}$$

where the plus and minus signs apply in the domains $x < 0$ and $x > 0$, respectively, and $a_i$ is an integration constant. In the bulk phases, the integration constant vanishes because $d\varphi/dx$ also does.

The other two constants, $a_{hc}$ and $a_m$, as well as the potentials $\varphi(-d_{hc})$, $\varphi(0)$, and $\varphi(d_m)$, are unknowns that have to be determined from the boundary conditions for the electric displacement

$$\epsilon_o \frac{d\varphi}{dx}\Big|_{x=-d_{hc}^-} = \epsilon_{hc} \frac{d\varphi}{dx}\Big|_{x=-d_{hc}^+} \tag{5a}$$

$$\epsilon_{hc} \frac{d\varphi}{dx}\Big|_{x=0^-} = \epsilon_m \frac{d\varphi}{dx}\Big|_{x=0^+} + \frac{F\sigma_0}{\epsilon_0 RT} \tag{5b}$$

$$\epsilon_m \frac{d\varphi}{dx}\Big|_{x=d_m^-} = \epsilon_w \frac{d\varphi}{dx}\Big|_{x=d_m^+} + \frac{F\sigma_m}{\epsilon_0 RT} \tag{5c}$$

and the integrals of eq 4 over the regions $i$ = hc and $i$ = m

$$\int_{\varphi(-d_{hc})}^{\varphi(0)} \frac{d\varphi}{[\kappa_{hc}{}^2 \sinh^2(\varphi/2) + a_{hc}]^{1/2}} = d_{hc} \quad (6a)$$

$$\int_{\varphi(0)}^{\varphi(d_m)} \frac{d\varphi}{[\kappa_m{}^2 \sinh^2((\varphi - \varphi_w^b)/2) + a_m]^{1/2}} = -d_m \quad (6b)$$

Once this equation system is solved, the surface charge density separated across the ITIES can be evaluated as

$$Q \equiv -\int_{-\infty}^{0} \rho dx = \frac{2\epsilon_0 RT}{F}\left[(\kappa_o\epsilon_o - \kappa_{hc}\epsilon_{hc}) \sinh\frac{\varphi(-d_{hc})}{2} + \kappa_{hc}\epsilon_{hc} \sinh\frac{\varphi(0)}{2}\right] \quad (7)$$

and the interfacial capacitance is calculated (by numerical differentiation) from eq 1.

## Experimental Section

**Materials.** The chemicals DOTAP (Sigma, ≥99%), methanol (Merck, p.a.), ethanol (ETAX Aa, Finland, 99.4%), 2-nitrophenyl octyl ether (*o*-NPOE, Fluka, Selectophore), poly(vinyl chloride) (PVC) (Sigma, very high molecular weight), chloroform (Merck, p.a.), tetraphenylarsonium chloride hydrate 97% (TPAsCl, Sigma, p.a.), potassium tetrakis-4-chlorophenylborate (KTPBCl, Aldrich, p.a.), sodium chloride (NaCl, Merck, p.a.), tetraethylammonium chloride hydrate ($TEACl{\cdot}H_2O$, Aldrich, p.a.), metaprolol tartrate (metoprolol, Sigma, reagent grade), hydrogen tetrachloroaurate tetrahydrate ($HAuCl_4{\cdot}4H_2O$, Sigma-Aldrich, 99.9+%), mercaptosuccinic acid (MSA, Aldrich, 97%), sodium borohydride ($NaBH_4$, Merck, for synthesis), dimethyldichlorosilane ($C_2H_6Cl_2Si$, Fluka, puriss >99.5%), PAH (Aldrich, molecular weight 70 kDa), and DS sodium salt from Leuconostoc ssp. (DS 500, Fluka, molecular mass 500 kDa), were all used as received without further purification. The buffer chemicals were potassium dihydrogen phosphate (J. T. Baker) and disodium hydrogen phosphate (Riedel-de Haën, p.a.). Millipore water (resistivity > 18 MΩ cm) was used to prepare all aqueous solutions and for rinsing. Figure 3 shows the chemical structure of PAH, DS, DOTAP, $TEA^+$, and metoprolol.

**Langmuir−Blodgett Films.** DOTAP dissolved in chloroform was used as a spreading solution. The typical solution concentration was 0.5 mg/mL. Surface pressure−molecular area ($\pi$−*A*) isotherms were measured with the computer-interfaced Langmuir trough (60 mm × 216 mm, KSV Instruments Ltd., Helsinki) in an earthed Faraday cage. The surface pressure was controlled with the platinum Wilhelmy plate, and the subphase was thermostated at 20.0 ± 0.1 °C. Lipid solutions were spread onto a sodium chloride aqueous subphase containing DS, drop by drop, with a Hamilton microliter syringe. After 30 min evaporation time, the isotherms were recorded at the compression speed of 5.0 mm/min. LB films were transferred by dipping the electrochemical cell perpendicularly through the lipid monolayer at the speed of 2.0 mm/min. The pressure equivalent to a bilayer is reported to be about 30−35 mN/m.[21,23] Therefore, the monolayer experiments in this work were carried out at the surface pressure of 32 mN/m. The success of the transfer was determined both from the electrochemical measurements and the so-called transfer ratio with values close to unit. No changes in the monolayers properties were observed over several hours even after being deposited at a liquid−liquid interface.

**AuNPs Preparation and Characterization.** Mercaptosuccinic acid stabilized AuNPs were synthesized as described in ref 12 using two different molar ratios, S/Au = 1.25 for particles of 1.7 nm, and S/Au = 0.5 for particles of 2.9 nm in average diameter. Briefly, 0.5 mmol of $HAuCl_4$ dissolved as 5% (w/v) aqueous solution was mixed with 1.25 mmol of MSA dissolved in 100 mL of methanol, resulting in a yellow transparent solution. Then, 0.2 M aqueous $NaBH_4$ solution was added under vigorous stirring at the rate of 5 mL/min. The solution turned dark brown immediately, and further addition of the reductant led to the formation of a flocculent dark-brown precipitate. After stirring for ca. 1 h, the solvent was decanted. To remove impurities, the remaining precipitate was centrifuged (Heraeus Sepatech Labofuge 200) five times for 15 min at 4500 rpm in the 20% (v/v) water/methanol solution and sonicated. Then the particles were washed, centrifuged, and sonicated in pure methanol to remove unbound MSA or Au−MSA complexes. Finally, the precipitate was suspended in ethanol and dried in a rotavapor at $T$ < 40 °C. The size distribution of the AuNPs was confirmed using a TEM (Tecnai G2), operating at 120 kV with a point resolution of 0.5 nm. The samples were prepared by adding droplets of the NP-containing aqueous solution on the copper−carbon grids and allowing them to dry in a drybox for ca. 24 h. The size distribution was estimated using free software, Image J.

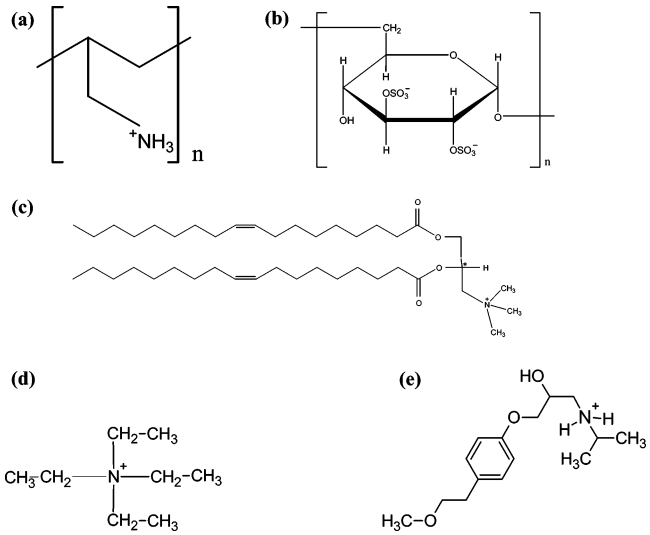


**Figure 3.** Chemical structures of PAH (a), DS represented in one of the three possible sulfate group forms (b), DOTAP (c), and $TEA^+$ (d) and metoprolol (e) in their cationic form. The asterisk (*) symbolizes the chiral center.

As a result of the $pK_{a1}$ and $pK_{a2}$ values of succinic acid,[42] 4.19 and 5.64, respectively, higher pH ensures the change of the carboxylic acid to its carboxylate ion form. Thus, the pH of the solution used in this work was about 6, which is the most appropriate to use for the electrostatic adsorption of the AuNPs in order to build up the multilayers. The pH range of 5.0−6.0 coincides with the ionization range of the mercaptosuccinic acid bound to gold as established by some authors.[43] Furthermore, the $pK_a$ of PAH is about 10, and hence, for pH 6, PAH is positively charged. All these parameters allow the easy construction of the multilayers and ensure their stability.

**Buildup of Multilayers.** PAH/AuNPs multilayers were built up by modifying slightly the method in ref 24. The electrochemical cell containing the organic gel was used as a substrate. After the transfer of the lipid−DS film on the substrate, the cell was kept in the well of the Langmuir trough. The volume of the aqueous solution was ca. 14 mL. The solution present inside the well was exchanged by pumping the 1 mg/mL PAH solution at the rate of 1.5 mL/min. The procedure was then repeated with 0.06 mg/mL AuNPs solution. To remove unbound AuNPs from the aqueous phase, the well was washed with the

**SCHEME 1**

| Ag | AgCl | 5 mM TPAsCl (w') | 10 mM TPAsTPBCl 5 w-% PVC (*o*-NPOE) | 15 mM NaCl + 1 mg/ml DS 500, *X* (w) | AgCl | Ag' |
|---|---|---|---|---|---|---|

15 mM NaCl solution. Thus, alternating layers of cationic PAH and anionic AuNPs were deposited up to a maximum of $n = 14$ layers. Multilayers with odd number of layers $n$ are terminated with a PAH layer, while those with even $n$ are terminated with a layer of AuNPs.

**Electrochemical Measurements.** AC impedance/voltammetry and cyclic voltammetry measurements were carried out with the Autolab 100 four-terminal potentiostat (EcoChemie B. V., Netherlands). The details of the cell construction and setup can be found elsewhere.[31,44] Briefly, the organic gel phase, a mixture of 5 wt % PVC and *o*-NPOE containing the base electrolyte, was heated at least to 110 °C, and the resulting hot gel was cast into the cell. Typically, the solidification of the gel was carried out overnight. NaCl was used as the aqueous base electrolyte and TPAsCl as the organic reference electrolyte. As described in detail elsewhere,[45] the organic base electrolyte TPAsTPBCl was obtained by precipitation from equimolar solutions of TPAsCl and KTPBCl. Ag/AgCl wires were used as reference electrodes and Pt wires as auxiliary electrodes for the electrochemical measurements.

The electrochemical cell used can be represented in Scheme 1, where $X$ is either $TEA^+$ or metoprolol at the concentration of about 50 $\mu$M. For the measurement of ion transfer, NaCl solutions were pumped into the cell after the washing stage, and hence, the AC voltammetric signal for each layer was recorded in NaCl solution.[24]

The cell interface with an area of 0.28 $cm^2$ was placed between two Luggin capillaries to minimize the ohmic drop. All electrochemical experiments were carried out at 20.0 ± 0.1 °C in a Faraday cage. Cyclic voltammograms were measured at the sweep rate of 10, 25, 50, 75, and 100 mV/s. AC voltammetry was measured at the frequency of 5, 10, 20, 25, and 30 Hz, using the sweep rate of 1 mV/s, an amplitude of 5 mV root-mean-square, with a modulation and interval time of 0.4 and 1 s, respectively. All measurements were carried out using 15 mM of NaCl as the aqueous solution and a DS concentration of 1 mg/mL, as described elsewhere.[22−23,46]

**Spectroscopic Measurements.** The multilayer growth was followed by UV−vis spectroscopy (HP 8452A diode array UV−vis spectrophotometry). Prior to multilayer assembly, the quartz slides were cleaned with the procedure described elsewere.[47] The quartz slides were then hydrophobized with dimethyldichlorosilane as follows.[4] The substrates were dipped for 5 min each in a sequence of methanol, methanol/chloroform (volume ratio 2:1), and chloroform solutions, respectively, under ultrasonication. Then they were kept for ca. 1 h at 30−40 °C in a solution of chloroform and dimethyldichlorosilane (volume ratio 2:1). Finally, the substrates were washed with chloroform and methanol/chloroform solutions (volume ratio 2:1). The DOTAP/DS monolayer was deposited onto the substrate via the LB technique. Finally, PAH/AuNPs layers were assembled by immersing the slide for 20 min in PAH (1 mg/mL) and AuNPs (0.06 mg/mL) solutions alternatively.

## Results and Discussion

**Isotherms.** Figure 4 shows the $\pi-A$ isotherms of DOTAP spread on different aqueous subphases: (A) 15 mM NaCl (solid line), (B) 15 mM NaCl + 0.06 mg/mL MSA-AuNPs (dashed line), and (C) 15 mM NaCl + 1.00 mg/mL DS (dotted line) at $T = 20.0 \pm 0.1$ °C. From the isotherms recorded at the air−liquid interface, the surface compressibility modulus, $C_s^{-1}$, can be calculated as

$$C_s^{-1} \equiv -A\left(\frac{\partial \pi}{\partial A}\right)_T \tag{8}$$

The isotherm of the DOTAP monolayer (curve A in Figure 4) in the absence of AuNPs and DS is characteristic for one single phase (a homogeneous liquid expanded fluid phase) and its compressibility modulus at 32 mN/m is 58 ± 3 mN/m. Especially at higher surface pressures, the DOTAP isotherms in the presence of AuNPs and DS are shifted toward larger areas per molecule. That is, for a given value of the surface pressure, the presence of AuNPs in the subphase makes the DOTAP monolayer more expanded, and this effect is even more noticeable in the presence of DS in the subphase. In the presence of AuNPs and DS, the compressibility modulus at 32 mN/m are 62 ± 2 and 118 ± 3 mN/m, respectively, indicating a lower compressibility that than of a pure DOTAP monolayer.

The negatively charged AuNPs and DS strands are electrostatically attached to the cationic lipid molecules. If the adsorbed negative charge is lower than the positive charge on the phospholipids, it should be expected that the DOTAP monolayer exhibits a lower molecular area (at fixed surface pressure) in the presence of AuNPs and DS in the subphase because of the weaker electrostatic repulsion among phospholipid headgroups. Because the opposite effect is observed, this might indicate that the positive charge is overcompensated and that adjacent adsorbed AuNPs and DS strands repel each other and lead to a more expanded monolayer. Finally, the results also suggest that the adsorbed AuNPs and DS do not penetrate the lipid monolayer[22] because no increase in the surface pressure at large molecular area was observed.

**Size Distribution of the AuNPs.** The AuNPs were characterized by using UV−vis and FT-IR spectroscopy (results not

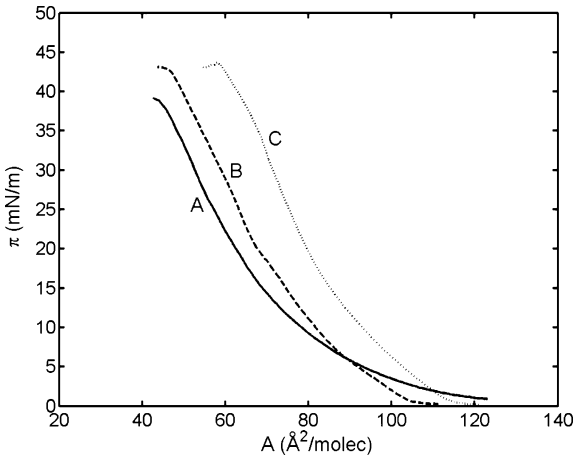


**Figure 4.** Isotherms of DOTAP spread on 15 mM NaCl (A, solid line), (B) 15 mM NaCl + 0.06 mg/mL MSA-AuNPs (B, dashed line), and 15 mM NaCl + 1.00 mg/mL DS (C, dotted line) at $T = 20.0 \pm 0.1$ °C.

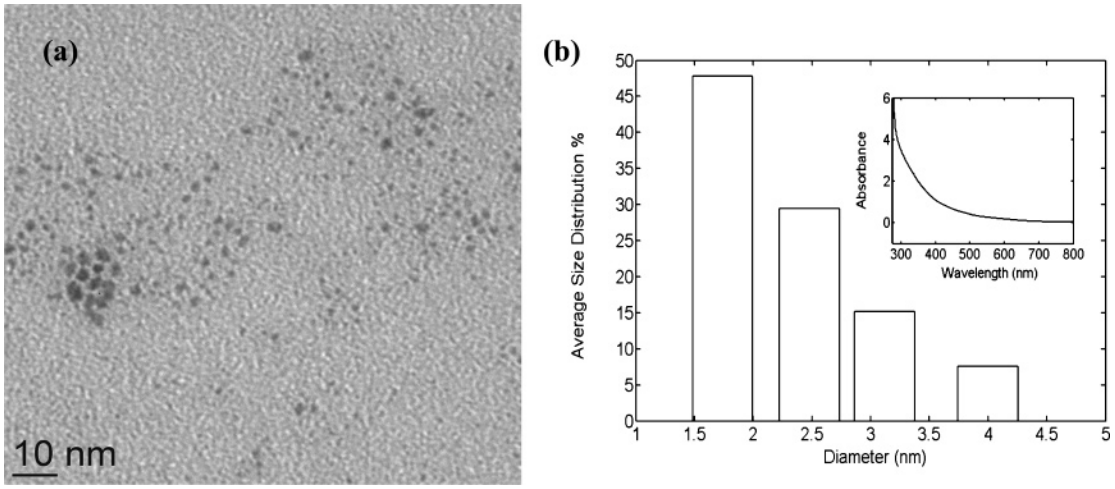


**Figure 5.** TEM image (left), and size distribution histogram (right) and UV−vis spectrum (inset) of AuNPs prepared with the molar ratio S/Au = 2.5.

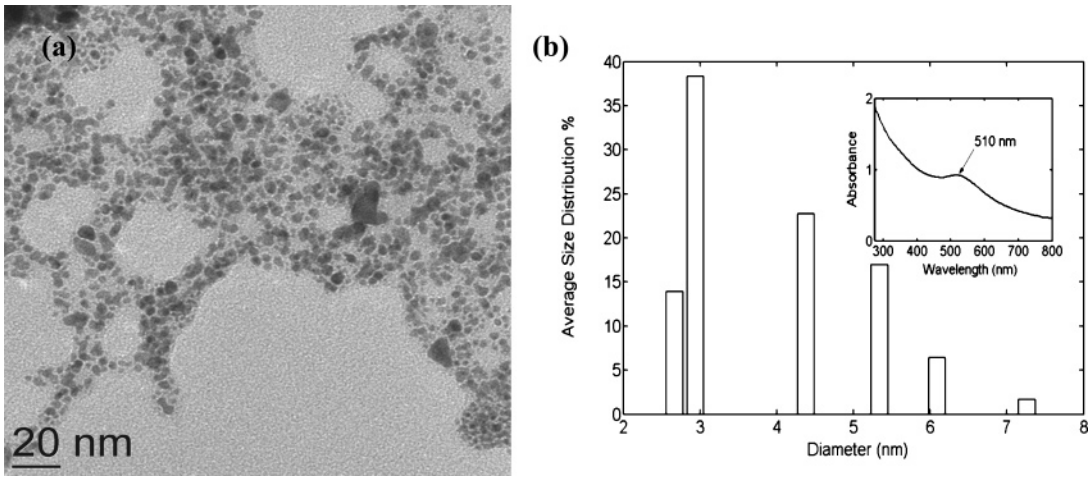


**Figure 6.** TEM image (left) and size distribution histogram (right) and UV−vis spectrum (inset) of AuNPs prepared with the molar ratio S/Au = 0.5.

shown), as well as TEM. Information about the size distribution and morphology of the AuNPs can be extracted from the TEM images. Figures 5 and 6 show the images (a), the size distribution histogram (b), and the UV−vis spectrum (inset) of AuNPs prepared at molar ratios (S/Au) of 2.5 and 0.5, respectively. The average diameters of the particles prepared with S/Au = 2.5 and 0.5, were 1.7 and 2.9 nm, respectively. The UV−vis spectra show typically no absorption peak for small AuNPs of an average size of 1.7 nm (orange-brown solutions were observed), and a broad surface plasmon band of about 510 nm for bigger NPs with average size of 2.9 nm. It is also observable that there is an increasing background in the optical spectra of the AuNPs in aqueous solution toward higher energy because of the Mie scattering from the particle suspension.[12,37,38] All these results are in good agreement with those observed elsewhere.[12]

It is known that the larger AuNPs are more stable in relation to TEM observation.[12] The particles with smaller diameter are difficult to observe, even under very weak electron beam radiation, and tend to aggregate. This structural instability can be due to the electron beam irradiation.[12]

**Spectroscopic Measurements.** The multilayer growth was followed by UV−vis absorption. The spectra of the multilayers at 510 nm are shown in Figure 7a and b as a function of the number of layers. The absorbance increases almost linearly with the number of layers, which indicates an excellent LbL assembling and is in good agreement with the literature.[12] This suggests that the multilayers are assembled uniformly, with each layer of AuNPs containing approximately the same amount of them. As expected, the AuNPs-terminated (Figure 7b) multilayers have a higher UV−vis absorbance. Similar results were obtained for the 1.7 nm AuNPs (results not shown), although in this case, the absorbance was lower and a less pronounced band at 510 nm was observed. Those results were also consistent with the previously cited studies.

**Capacitance Studies.** The interfacial capacitance, *C*, of the composite interfacial nanostructure was measured by using AC voltammetry. Because the kinetics of ion transfer across the interfacial nanostructure is rather fast, its equivalent circuit can be given as the parallel combination of a capacitor and the Warburg impedance. Hence, the admittance of the interface is

$$Y = \frac{\sqrt{j\omega}}{\sigma_W} + j\omega C \tag{9}$$

where $\omega$ is the angular frequency of the applied ac signal and $\sigma_W$ is the coefficient of the Warburg impedance. Thus, the capacitance can be calculated from[48]

$$\omega C = Y'' - Y' \tag{10}$$

where $Y''$ and $Y'$ are the imaginary and the real components of the admittance, respectively.

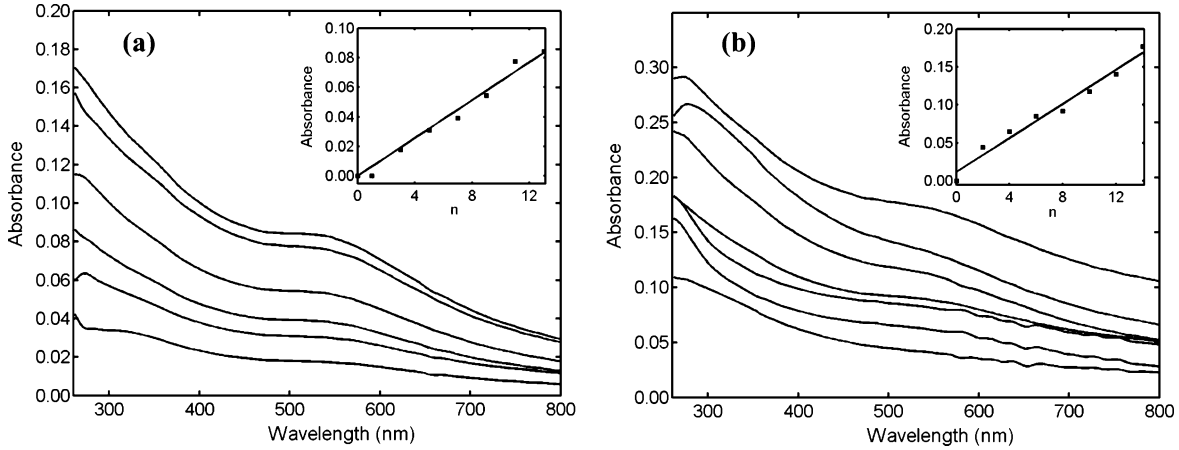


**Figure 7.** UV−vis spectra of PAH-terminated multilayers (3, 5, 7, 9, 11, and 13 layers from bottom to top) (a), and 2.9 nm AuNPs-terminated multilayers (2, 4, 6, 8, 10, 12, and 14 layers from bottom to top) (b). Insets: absorbance at 510 nm versus the number of layers. No UV−vis absorbance was observed from the DOTAP/DS and DOTAP/DS/PAH complexes.

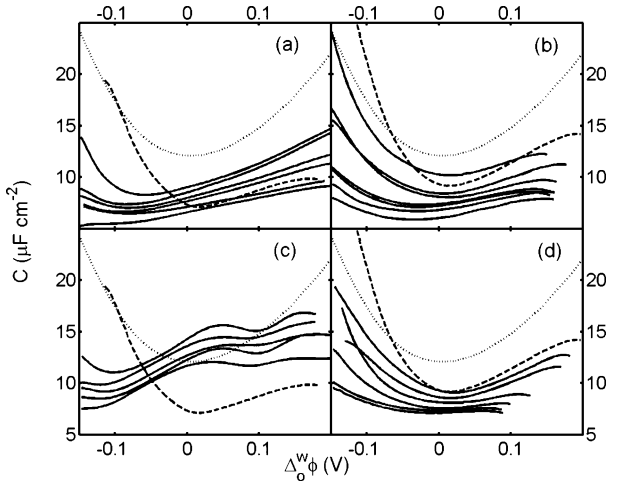


**Figure 8.** Experimental capacitance curves of multilayers containing 1.7 nm (a and b) and 2.9 nm AuNPs (c and d): (a) $n = 1$ (dashed line), 3, 5, 7, 9, 11, and 13 layers (solid lines from top to bottom); (b) DOTAP/DS monolayer (dashed line) and multilayers with $n = 2$, 4, 6, 8, 10, 12, and 14 layers (solid lines from top to bottom); (c) $n = 1$ (dashed line), 3, 5, 7, 9, and 11 layers (solid lines from top to bottom); and (d) DOTAP/DS monolayer (dashed line) and multilayers with $n = 2$, 4, 6, 8, 10, and 12 layers (solid lines from top to bottom). A clean interface (dotted line) is also shown in all cases for comparison.

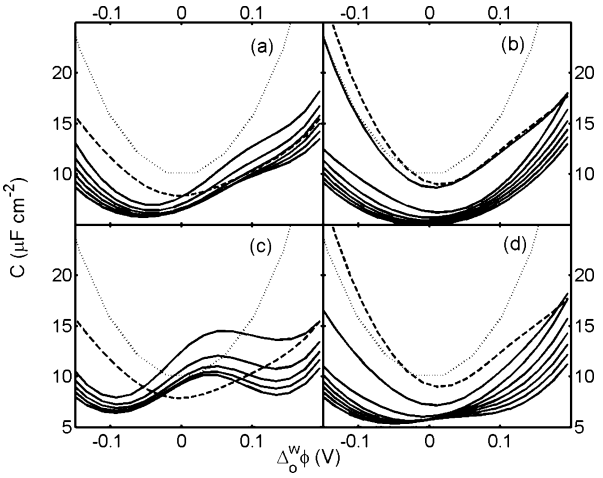


**Figure 9.** Calculated capacitance curves of multilayers containing 1.7 nm (a and b) and 2.9 nm AuNPs (c and d): (a) $n = 1$ (dashed line), 3, 5, 7, 9, 11, and 13 layers (solid lines from top to bottom); (b) DOTAP/DS monolayer (dashed line) and multilayers with $n = 2$, 4, 6, 8, 10, 12, and 14 layers (solid lines from top to bottom); (c) $n = 1$ (dashed line), 3, 5, 7, 9, and 11 layers (solid lines from top to bottom); and (d) DOTAP/DS monolayer (dashed line) and multilayers with $n = 2$, 4, 6, 8, 10, and 12 layers (solid lines from top to bottom). A clean interface (dotted line) is also shown in all cases for comparison.

First, the capacitance-potential curves were measured for the clean and for the DOTAP/DS-covered interface. Then, alternate layers of PAH and AuNPs were deposited as described above, and the AC voltammetric response was recorded.

Figure 8a shows the capacitance curves corresponding to PAH-terminated multilayers as well as that of the clean interface for comparison. The curves for 1.7 nm AuNPs-terminated multilayers are shown in Figure 8b. The shift of the potential of minimum capacitance in the curve for the DOTAP/DS monolayer with respect to that of the clean interface may be attributed to the dipole moment of the phospholipid molecules.[24,31,49] In the case of multilayers, a shift in the capacitance curves either to more negative (PAH-terminated) or positive potentials (AuNPs-terminated multilayers) was observed. Similar results were obtained by Slevin et al.[24] using PAH and PSS as cationic and anionic polyelectrolytes, respectively. After the deposition of the first PAH layer, a small decrease of the capacitance (with respect to that of the DOTAP/DS monolayer) is observed. The deposition of the first AuNPs layer increases the capacitance, and the next PAH layer causes a much larger reduction in capacitance. In general, for a given termination type, the capacitance decreases as the number of layers increases.

Similar results obtained with 2.9 nm AuNPs are presented in Figure 8c and d. In this case, only 12 layers were deposited, because further increase in the number of layers did not led to significant changes in the capacitance curves of the AuNPs-terminated multilayers. On the other hand, the PAH-terminated multilayers show a different behavior. The overall capacitance values are slightly higher compared to those in Figure 8a. More interestingly, another minimum in the capacitance curves is observed at ca. 0.1 V.

Similar capacitance curves are calculated using the above theoretical model. In all calculations, the relative permittivities of the aqueous and organic solutions are[22] $\epsilon_w = 78.54$ and $\epsilon_o = 24.2$, respectively, and that of the multilayer has been estimated as[24] $\epsilon_m = 45$. The ratio $\epsilon_{hc}/d_{hc}$ has been fixed to 1 $nm^{-1}$. For $n > 1$, the thickness of the multilayer has been evaluated as $d_m = nd_0$, where $n$ is the number of layers. The average value for the layer thickness is $d_0 = 0.74$ nm when 1.7 nm AuNPs are used, and 1.10 nm in the case of 2.9 nm AuNPs.

**TABLE 1: Values of the Theoretical Parameters for the DOTAP/DS Monolayer without and with the First PAH Layer ($n = 1$)[a]**

| | $d_m$ (nm) | $K_m$ | α | $\gamma$ |
|---|---|---|---|---|
| DOTAP/DS | 2.2 | 0.864 | 0.01 | −3.0 |
| DOTAP/DS/PAH | 0.75 | 0.1 | −0.04 | 0.07 |

[a] $K_{hc} = 1.0$ in both cases.

**TABLE 2: Values of the Theoretical Parameters for the PAH-Terminated (*n* Odd) and the AuNPs-terminated (*n* Even) Multilayers**

| | 1.7 nm average size | | | 2.9 nm average size | | |
|---|---|---|---|---|---|---|
| *n* | $K_{hc}$ | $K_m$ | α | $K_{hc}$ | $K_m$ | α |
| 2 | 1.0 | 0.75 | 0.01 | 1.0 | 0.75 | 0.02 |
| 3 | 0.4 | 1.00 | 0.01 | 1.0 | 0.40 | 0.04 |
| 4 | 0.3 | 0.77 | 0.01 | 0.8 | 0.38 | 0.02 |
| 5 | 0.3 | 0.92 | 0.02 | 0.7 | 0.36 | 0.04 |
| 6 | 0.2 | 0.70 | 0.01 | 0.6 | 0.34 | 0.02 |
| 7 | 0.2 | 0.84 | 0.02 | 0.6 | 0.32 | 0.04 |
| 8 | 0.2 | 0.64 | 0.01 | 0.5 | 0.30 | 0.02 |
| 9 | 0.1 | 0.76 | 0.02 | 0.5 | 0.28 | 0.04 |
| 10 | 0.1 | 0.58 | 0.01 | 0.4 | 0.26 | 0.02 |
| 11 | 0.1 | 0.68 | 0.02 | 0.4 | 0.24 | 0.04 |
| 12 | 0.1 | 0.51 | 0.01 | 0.3 | 0.22 | 0.02 |
| 13 | 0.1 | 0.60 | 0.03 | | | |
| 14 | 0.1 | 0.45 | 0.01 | | | |

The model also includes the parameters $K_{hc}$, $K_m$, α, and $\gamma$, which have been varied in the calculations. The chemical partition coefficients $K_{hc}$ and $K_m$ account for the differences in electrical permittivities, as well as any other nonidealities such as finite size effects of the ions (volume exclusion). The dimensionless surface charge densities at $x = 0$ and $x = d_m$ are simplified representations of the complex distribution of bound charges in the composite multilayer. Because DOTAP is a positively charged phospholipid, the charge density α at $x = 0$ is expected to be positive. This is an effective value that somehow takes into account the presence of the negative DS chains bound to the phospholipids headgroups, and therefore, the value of α is much lower than 1. The dimensionless surface charge density $\gamma$ at $x = d_m$ is influenced by the DS layer and the different PAH and AuNPs layers. It should be positive for PAH-terminated multilayers (i.e., *n* odd) and negative for AuNPs-terminated multilayers (i.e., *n* even). Thus, in the case of 1.7 nm AuNPs, we have used $\gamma = 0.1$ for PAH-terminated multilayers and $\gamma = -0.1$ for AuNPs-terminated ones. In the case of 2.9 nm AuNPs, the corresponding values are 0.2 and −0.3.

The cases of an uncovered DOTAP/DS monolayer and $n = 1$, when a single PAH layer is deposited, require special consideration. DS binds strongly to DOTAP, but there are unbounded loose chains and the structure is not compact. This is reflected both on the thickness of the layer and the high value for the partition coefficient $K_m$. The latter is consistent with previous attenuated total reflection measurements[22] in which binding of DS to other phospholipids headgroups was considered. It was then found that the layer of the absorbed DS contained a significant amount of water, and hence, a significant concentration of small mobile ions coming from the aqueous phase is also expected. The unbounded DS chains contribute to lower the value of $\gamma$. In light of theoretical simulation of the capacitance curves, when the first PAH layer is deposited, the thickness of the DOTAP/DS/PAH nanostructure seems to decrease compared to that of the DOTAP/DS monolayer. This is also reflected in a lower value for $K_m$, which can be related to volume exclusion of the base electrolyte ions. Adding the PAH layer thus has an effect similar to compression of the DOTAP/DS monolayer. DS binds then more effectively to DOTAP, and the effective surface charge density α at $x = 0$ becomes negative in this case. At $x = d_m$, the surface charge $\gamma$ is positive, however, allowing for the deposition of the following negative AuNPs layer.

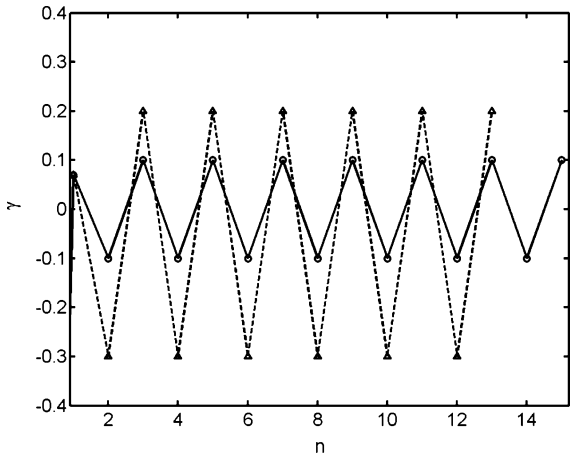


**Figure 10.** Dimensionless surface charge density $\gamma$ employed in the calculations as a function of the number of layers (*n*) for 1.7 nm (circles) and 2.9 nm AuNPs (triangles). Lines are guides for the eye. The DOTAP/DS monolayer (not shown) has $\gamma = -3.0$.

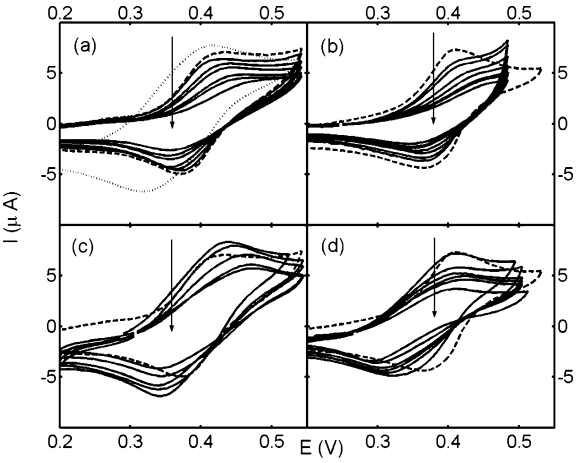


**Figure 11.** CVs of metoprolol transfer at the scan rate of 50 mV/s: with $n$=1 (dashed line), 3, 5, 7, 9 and 11 PAH-terminated layers from the top to the bottom (a) and (c) (1.7 and 2.9 nm AuNPs, respectively); with DS (dashed line), 2, 4, 6, 8, 10, and 12 AuNPs-terminated layers from the top to the bottom (b) and (d) (1.7 and 2.9 nm AuNPs, respectively). In (a), the CV for a DOTAP/DS layer (dotted line) is also shown.

Figure 9 shows the calculated capacitance curves. The values for the theoretical parameters are given in Tables 1 and 2. The value of the surface charge density $\gamma$ is plotted in Figure 10.

The shift of the minimum in the capacitance curves to more negative or positive potentials is governed by the more positive or negative values of $\gamma$, respectively, consistent with the previous findings by Slevin et al.[24] However, here, the surface charge density α also contributes. The positive values of α control the position of the minimum at negative potentials in the case of PAH-terminated layers. The effect of α is noticed also in the gradual shift of the minimum to more negative values observed for AuNPs-terminated multilayers as *n* increases. Moreover, α is responsible for the great change in the capacitance observed after the first PAH layer is deposited because it then becomes positive (maybe because some DS chains are released) and shifts the minimum to more negative potentials.

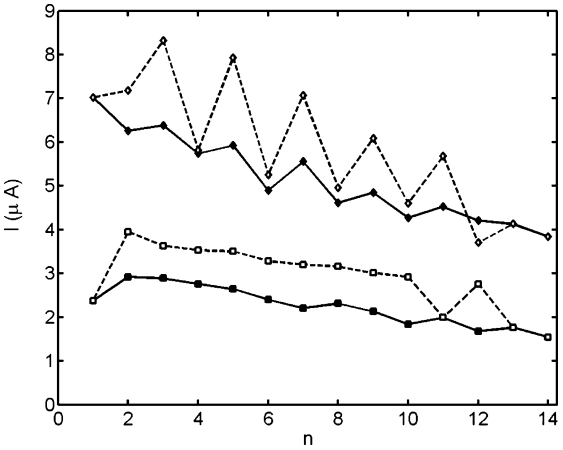


**Figure 12.** Peak current vs number of layers (*n*) for the ion transfer across the PAH/AuNPs assemblies; NPs of 1.7 nm (solid line) and 2.9 nm (dashed line), $TEA^+$ (■, □) and metoprolol (◆, ◇).

It should be noted that α is usually higher for PAH-terminated multilayers. This is due to the fact that the deposition of the outer positive PAH layer leads to a release of some negative charges from the plane $x = 0$: the complexation affects the whole structure of the multilayer, and a change in the outer layers propagates to the previously deposited ones. The change of α is more significant for multilayers containing 2.9 nm AuNPs, suggesting that these multilayers are more fuzzy. The values of α are also generally higher in this case, suggesting a slightly weaker absorption, as observed in the experimental curves.

The capacitance decreases as the thickness of the multilayer increases. Roughly, the features of the hydrocarbon layer and the multilayer become important at negative and positive potentials, respectively. The decrease of $K_m$ tends to decrease the capacitance at positive potentials, and lower values for $K_{hc}$ are related to lower capacitance values at negative potentials. $K_{hc}$ decreases with increasing *n*, which means that there is a higher exclusion of ions from the organic phase in the hydrocarbon layer. This can be due to a change in the tilt angle of the hydrophobic tails as a consequence of the nature of the binding to the multilayer, leading to a more dense structure with lower free volume available for ions from the organic phase. $K_m$ decreases monotonically for multilayers with 2.9 nm AuNPs, reflecting ion exclusion due to an increasingly and homogeneously compact structure. For multilayers with 1.7 nm, AuNPs $K_m$ also decreases with *n* but its value oscillates depending on the charge of the last layer. This probably reflects certain degree of stratification of the multilayer. This structuration is consistent with the discussion given above concerning the changes of α for these multilayers.

The relative minimum observed in the experiments at about 0.1 V is reproduced by the calculations slightly displaced to ca. 0.13 V (see Figure 9c). The relative minimum at these positive potentials is due to the lower values of $K_m$ and the higher absolute values of α and $\gamma$ that exhibit the multilayers containing 2.9 nm AuNPs compared to those of 1.7 nm. For lower $K_m$, the concentration of ions coming from the aqueous phase is also lower, and this tends to make the contribution of the surface charge excess at $x = d_m$ more important. Furthermore, because this plane now has a higher absolute value for the charge, its contribution to the capacitance is still higher. This leads to a better distinction of the contributions due to the multilayer (positive potentials) and to the hydrocarbon chains (negative potentials).

Finally, it should be noted that our model tends to overestimate the capacitance close to the positive edge of the potential window. This is clearly seen in the case of a clean interface. For an interfacial potential of 0.15 V, the model predicts a capacitance of 25 $\mu$F cm$^{-2}$, which is higher than the experimental value of about 17 $\mu$F cm$^{-2}$. Still, the model reproduces the essential trends of the capacitance curves.

**Ion Transfer Studies.** To study ion transfer across the interfacial nanostructures, cyclic voltammograms (CVs) were measured with $TEA^+$ and the cationic drug, metoprolol, as the transferring probe ions. Figure 11 shows the CVs for the ion transfer of metoprolol across the DOTAP/DS monolayer, deposited at surface pressure of 32 mN/m, in the absence and in the presence of PAH/AuNPs multilayers. The nanoparticle size influences significantly the CV response, as we can see by comparison of Figure 11a and b (1.7 nm) and Figure 11c and d (2.9 nm).

The peak currents are summarized in Figure 12. In general, the multilayers were very stable during the electrochemical measurements, i.e., the anodic and cathodic peak currents were unchanged during repeated cycling even over 24 h. As can be seen, the peak separation increases with the number of layers, and the peak separation is greater in the presence of 2.9 nm AuNPs. In general, the peak current decreases with increasing *n*, which is plausible, as the layers must present a transfer barrier. The effect seems to be higher in the presence of metoprolol

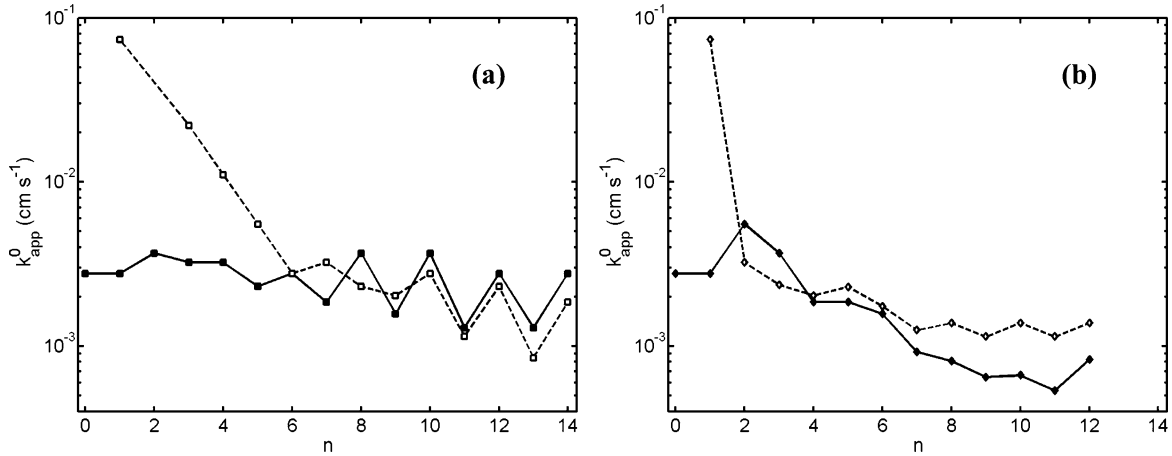


**Figure 13.** Apparent rate constants of $TEA^+$ (■, ◆) and metoprolol (□, ◇) transfer across the interfacial composite nanostructures as a function of the number of layers (*n*) for 1.7 nm (a) and 2.9 nm AuNPs (b).

than $TEA^+$. In some cases, the change on the CV peaks can also be explained due to the nonuniform size distribution of the NPs.

Before each ion transfer measurement, voltammograms were corrected by subtracting the current due to the base electrolytes only. The peak currents for the transfer for both cations across the DOTAP/DS monolayer in the absence and in the presence of PAH/AuNPs multilayers were approximately proportional to the square root of the scan rate (results not shown). Hence, it can be concluded that the ion transfer is under mixed kinetic and diffusion control and the kinetic parameters can then be determined by using Nicholson's method, i.e., by applying the following equation[50]

$$\psi = \frac{\left(\frac{D_w}{D_o}\right)^{\alpha/2} k^0_{app}}{[\pi D_w f \nu]^{1/2}} \tag{11}$$

where $f = nF/RT$, $D_w$ and $D_o$ are the water and the oil diffusion coefficients of the transferring ion, respectively, $\alpha \approx 0.5$ is the transfer coefficient, and $\nu$ is the scan rate.

By using the values from ref 22, the kinetic parameter, $\psi$, can be related to the peak separation by calculating $\psi$ at each scan rate for each layer, and the effective rate constant, $k^0_{app}$, for the ion transfer can be determined by peak separation. Before each ion transfer measurement, CVs were corrected by subtracting the response recorded in a solution containing base electrolytes only. The diffusion coefficients $D_w$ and $D_o$ of $TEA^+$ and metoprolol obtained for a PVC gel phase were reported to be $1.0 \times 10^{-5}$ and $4.8 \times 10^{-7}$ $cm^2\ s^{-1}$, and $5.9 \times 10^{-6}$ and $1.3 \times 10^{-7}$ $cm^2\ s^{-1}$, respectively, for the aqueous−organic gel interface.[31] As a result of the similarity of our system relative to those authors, the same parameters were used to calculate the effective rate constant. Figure 13 shows the apparent rate constants for $TEA^+$ and metoprolol transfer, calculated from the CVs by applying eq 11, as a function of the number of layers.

Because both cations are singly charged, a similar behavior might be expected for their transfer. However, because of the magnitude of the difference between the transfer across the PAH- and AuNPs-terminated layers, as well as the double-layer effects,[51] the apparent rate constant for negatively and positively charged surfaces is expected to be different because of their different transfer potentials.[24] The ion transfer through the polyelectrolyte/AuNPs composite multilayers was slightly faster than in other studies carried out using polyelectrolyte multilayers.[24] This is attributed to both the presence of AuNPs and the DS coupled to the phospholipid monolayer.[22]

## Conclusions

In this work we have shown that AuNPs can be used as charged species in film fabrication by alternating with oppositely charged polyelectrolytes. Stable PAH/AuNPs multilayers with up to 14 layers were successfully assembled on a DOTAP/DS hybrid layer at an aqueous−organic gel interface by combination of LB and LbL techniques. We have studied both experimentally and theoretically the interfacial capacitance of the composite multilayers. It has been shown that the decrease of the overall capacitance with the number of layers is due to the increasing thickness as well as to the decreasing partition coefficients of the supporting electrolytes in the hydrocarbon region and the multilayer. It is found that the potential of minimum capacitance shifts to more negative values for PAH-terminated multilayers while the contrary is observed for AuNPs-terminated ones. The excellent agreement between theoretical and experimental capacitance curves allows us to conclude that these nanocomposites behave similarly to polyelectrolyte multilayers, with the outmost layer determining the alternating sign of the outer surface charge density. The absolute value of this outer charge density is much larger than that close to the cationic phospholipids and is observed to increase with the size (and charge) of the AuNPs. Finally, the CVs are used to evaluate the transfer rate constant across the multilayers of a model cationic drug, metoprolol, and the standard probe tetraethylammonium ion. The observed rate constants are slightly larger than in other studies using polyelectrolyte multilayers and decrease with an increasing number of layers.

**Acknowledgment.** Financial support from the European Union under the research and training network SUSANA ("Supramolecular Self-Assembly of Interfacial Nanostructures", contract number HPRN-CT-2002-00185) is gratefully acknowledged. H. A. Santos would like to thank Timo Laaksonen for technical assistance with TEM images. Dr. Lasse Murtomäki is also acknowledged for helpful discussions. J.A.M. and V.G.M. also thank the Ministry of Science and Technology of Spain and the European Union (FEDER funds) for the financial support under the DGICYT project number MAT2002-0646.

## References and Notes

(1) Templeton, A. C.; Wuelfing, W. P.; Murray, R. W. *Acc. Chem. Res.* **2000**, *33*, 27−36.
(2) Fendler, J. H. *Chem. Mater.* **2001**, *13*, 3196−3210.
(3) Decher, G. *Science* **1997**, *277*, 1232−1237.
(4) Schuetz, P.; Caruso, F. *Colloids Surf., A* **2002**, *207*, 33−40.
(5) Hicks, J. F.; Seok-S. Y.; Murray, R. W. *Langmuir* **2002**, *18*, 2288−2294.
(6) Cant, N. E.; Zhang, H.-L.; Critchley, K.; Mykhalyk, T. A.; Davies, G. R.; Evans, S. D. *J. Phys. Chem. B* **2003**, *107*, 13557−13562.
(7) Ferreyra, N.; Coche-Guérente, L.; Fatisson, J.; Teijelo, M. L.; Labbé, P. *Chem. Commun.* **2003**, 2056−2057.
(8) Ruiz, V.; Liljeroth, P.; Quinn, B. M.; Kontturi, K. *Nano Lett.* **2003**, *3*, 1459−1462.
(9) Tian, S.; Liu, J.; Zhu, T.; Knoll, W. *Chem. Commun.* **2003**, 2738−2739.
(10) Sennerfors, T.; Bogdanovic, G.; Tiberg, F. *Langmuir* **2002**, *18*, 6410−6415.
(11) *Colloidal Gold: Principles, Methods and Applications*; Hayat, M. A., Ed.; Academic Press: San Diego, CA, 1989; Vols. 1 and 2.
(12) Chen, S.; Kimura, K. *Langmuir* **1999**, *15*, 1075−1082.
(13) Brust, M.; Walker, M.; Bethell, D.; Schiffrin, D. J.; Whyman, R. *J. Chem. Soc., Chem. Commun.* **1994**, 801−802.
(14) Johnson, S. R.; Evans, S. D.; Mahon, S. W.; Ulman, A. *Langmuir* **1997**, *13*, 51−57.
(15) Ingram, R. S.; Hostetler, M. J.; Murray, R. W. *J. Am. Chem. Soc.* **1997**, *119*, 9175−9178.
(16) Brown, L. O.; Hutchison, J. E. *J. Am. Chem. Soc.* **1997**, *119*, 3921−3926.
(17) Shai, Y. *Biochim. Biophys. Acta* **1999**, *1462*, 55−70.
(18) Eum, K. M.; Langley, K. H.; Tirrell, D. A. *Macromolecules* **1989**, *22*, 2755−2760.
(19) Thomas, J. L.; Tirrel, D. A. *J. Controlled Release* **2000**, *67*, 203−209.
(20) de Meijere, K.; Brezesinski, G.; Möhwald, H. *Macromolecules* **1997**, *30*, 2337−2342.
(21) Huster, D.; Paasche, G.; Dietrich, U.; Zschörnig, O.; Gutberlet, T.; Gawrish, K.; Arnold, K. *Biophys. J.* **1999**, *77*, 879−887.
(22) Santos, H. A.; García-Morales, V.; Roozeman, R.-J.; Manzanares, J. A.; Konturri, K. *Langmuir* **2005**, *21*, 5475−5484.
(23) de Meijere, K.; Brezesinski, G.; Zschörnig, O.; Arnold, K.; Möhwald, H. *Physica B* **1998**, *248*, 269−273.
(24) Slevin, C. J.; Mälkiä, A.; Liljeroth, P.; Toiminen, M.; Kontturi, K. *Langmuir* **2003**, *19*, 1287−1294.
(25) Kakiuchi, T.; Kondon, T.; Kotani, M.; Senda, M. *Langmuir* **1992**, *8*, 169−175.
(26) Kontturi, A.-K.; Kontturi, K.; Murtomäki, L.; Quinn, B.; Cunnane, V. J. *J. Electroanal. Chem.* **1997**, *424*, 69−74.

(27) Wandlowski, T.; Marecek, V.; Samec, Z. *J. Electroanal. Chem.* **1988**, *242*, 277−290.
(28) Koryta, J. *Electrochim. Acta* **1979**, *24*, 293−300.
(29) Mälkiä, A.; Liljeroth, P.; Kontturi, K. *Electrochem. Commun.* **2003**, *5*, 473−479.
(30) Mälkiä, A.; Liljeroth, P.; Kontturi, K. *Anal. Sci.* **2001**, *17*, i345−i348.
(31) Mälkiä, A.; Liljeroth, P.; Kontturi, A.-K.; Kontturi, K. *J. Phys. Chem. B* **2001**, *105*, 10884−10892.
(32) Radhakrishnamurthy, B.; Ruitz, H. A.; Srinivasan, S. R.; Preau, W.; Dalferes, E. R.; Berenson, G. S. *Atherosclerosis* **1978**, *31*, 217−229.
(33) Bangham, A. D.; Hill, M. W.; Miller, N. G. A. *Science* **1988**, *240*, 646−649.
(34) Ruponen, M.; Ylä-Herttuala, S.; Urtti, A. *Biochim. Biophys. Acta* **1999**, *1415*, 331−341.
(35) Wiethoff, C. M.; Smith, J. G.; Koe, G. S.; Middaugh, C. R. *J. Biol. Chem.* **2001**, *276*, 32806−32813.
(36) Ruponen, M.; Honkakoski, P.; Tammi, M.; Urtti, A. *J. Gene Med.* **2004**, *6*, 405−414.
(37) Chen, S. *Langmuir* **2001**, *17*, 2878−2884.
(38) Chen, S. *Langmuir* **2001**, *17*, 6664−6668.
(39) Collier, C. P.; Saykally, R. J.; Shiang, J. J.; Henrichs, S. E.; Heath, J. R. *Science* 1**997**, *277*, 1978−1981.
(40) Yi, K. C.; Hórvölgyi, Z.; Fendler, J. H. *J. Phys. Chem.* **1994**, *98*, 3872−3881.
(41) Heath, J. R.; Knobler, C. M.; Leff, D. V. *J. Phys. Chem. B* **1997**, *101*, 189−197.
(42) Wade, L. G., Jr. *Organic Chemistry*; Prentice Hall: New York, 1987; p 978.
(43) Maya, L.; Stevenson, K. A.; Muralidharan, G.; Thundat, T. G.; Kenik, E. A. *Langmuir* **2002**, *18*, 2392−2397.
(44) Liljeroth, P.; Mälkiä, A.; Cunnane, V.; Kontturi, A.-K.; Kontturi, K. *Langmuir* **2000**, *16*, 6667−6673.
(45) Cunnane, V. J.; Schiffrin, D. J.; Beltran, C.; Geblewicz, G.; Solomon, T. *J. Electroanal. Chem.* **1988**, *247*, 203−214.
(46) Zschörnig, O.; Richter, W.; Paasche, G.; Arnold, K. *Colloid Polym. Sci.* **2000**, *278*, 637−646.
(47) Decher, G.; Hong, J. D. *Thin Solid Films* **1992**, *210*, 831−835.
(48) Kakiuchi, T.; Senda, M. *Collect. Czech. Chem. Commun.* **1991**, *56*, 112−129.
(49) Kakiuchi, T.; Nakanishi, M.; Senda, M. *Bull. Chem. Soc. Jpn.* **1989**, *62*, 403−409.
(50) Nicholson, R. S. *Anal. Chem.* **1965**, *37*, 1351−1355.
(51) Manzanares, J.; Allen, R. A.; Kontturi, K. *J. Electroanal. Chem.* **2000**, *483*, 188−201.